Hollow Fiber Membrane Contactor for Hydrogen Sulfide Odor Control

Noureddine Boucif, Eric Favre, and Denis Roizard
Laboratoire des Sciences du Génie Chimique, (UPR CNRS 6811) Nancy Université,
ENSIC-BP 451 1, rue Grandville, F-54001 Nancy Cedex, France

Mohamed Belloul
Dépt. de Chimie, Université de Mostaganem, Mostaganem 27000, Algeria

DOI 10.1002/aic.11348
Published online November 9, 2007 in Wiley InterScience (www.interscience.wiley.com).

Hollow fiber membrane modules are extensively used as gas–liquid contactors for acid gas removal from waste gas streams. Hydrogen sulfide is an important indoor and outdoor contaminant, but, given its toxicity, a limited number of experimental results have been reported for this compound. Moreover, chemical absorption has been exclusively investigated. In this study, hydrogen sulfide odor control by absorption in water thanks to a hollow fiber contactor has been studied both experimentally and theoretically. The scrubbing of hydrogen sulfide from air gas mixture is investigated in two porous polypropylene (PP) hollow fiber modules of different contact area and fiber packing fraction. The gas phase is circulated in the lumen of the fiber bore and the liquid phase in the shell in a nonwetted mode, i.e. the membrane pores being filled with gas. The gas phase was run in countercurrent contact with the liquid phase at constant pressure. A laminar parabolic velocity has been employed to describe the convective diffusive mass transport equation which has been solved analytically and numerically. The calculated extents of hydrogen sulfide depletion reasonably compare with the generated experimental results for both membrane modules. Up to 85% of acid gas could be removed at gaseous flowrates of 200 cm^3/min for the large module and removals as high as 89% at 10 cm^3/min have been observed for the smaller one. The overall mass-transfer coefficients calculated from the experimental data, agree satisfactorily with those generated by the mathematical model. The relation of the dimensionless Sherwood number to the Graetz number is in a good agreement with the Levêque semianalytical solution. © 2007 American Institute of Chemical Engineers *AIChE J,* 54: 122–131, 2008

Keywords: absorption, membrane separations, gas purification, mathematical modeling

Introduction

Membrane-based gas–liquid contactors have known in the last decade a considerable development. This technology has proven attractive for numerous applications in two broad areas, namely, the biological treatment of contaminated gas streams (trichloroethylene, propene, and other VOC's), and the abiotic gas absorption of waste gases (sulfur dioxide, ammonia, etc.). The first reported application of this membrane-based gas–liquid absorption process was the blood oxygenation using a hydrophobic flat PTFE film where blood flows in one side and air or pure oxygen on the other side of the membrane.[1] Different authors[2–4] have used later microporous hollow fiber

Correspondence concerning this article should be addressed to E. Favre at Eric.Favre@ensic.inpl-nancy.fr.
N. Boucif: On sabbatical leave from the Département de Chimie Industrielle et LPQ3M, Université de Mascara, Mascara 29000, Algérie.

membranes devices to study the absorption of a number of gases (carbon dioxide, sulfur dioxide, ammonia, etc.) into various solvents or aqueous solutions (water, soda, MEA, etc.).

These devices resemble shell and tube heat exchangers as far as the configuration is concerned. The only difference is that in the hollow fiber membrane contactor, the fibers are randomly bundled and potted in the shell cartridge, whereas in heat exchangers, the tubes are arranged in a well defined geometrical pitch.

Even though conventional absorption processes (bubble columns, packed and spray towers) have been used in the chemical industry for decades, the interdependence of the fluids to be contacted presents a real disadvantage that sometimes results in difficulties such as foaming, flooding, and emulsions. The gas–liquid hollow fiber membrane contactor (HFMC) has proven to be a promising technique to overcome these shortcomings. Besides the nondispersive contact between fluids, this technique offers a larger, and easy to evaluate, interfacial contact area. Matson et al.[5] reported that surface contact area developed by a fiber module could reach 8000 m^2/m^3 whereas in conventional absorption towers, it is only of 800 m^2/m^3. Yang and Cussler[6] have observed a 10-fold increase in efficiency when using a hollow fiber module over a conventional absorption packed column.

However, the presence of a membrane itself consists of another resistance to mass transfer, which is not encountered in absorption columns. This resistance could negatively affect the overall mass transfer and significantly lower the selectivity. This membrane resistance can be minimized by reducing the membrane thickness or by increasing its intrinsic gas permeability. Many authors[2,7] have specifically investigated this point.

Membrane contactors-based processes have been reviewed very concisely by Sirkar,[8] and thoroughly detailed by Gabelman and Hwang.[9]

For gas–liquid contact devices, two types of membranes can be used: hydrophobic microporous polymer material such as polypropylene and dense polymeric material such as silicone rubber (polydimethylsiloxane). The microporous material presents a higher permeability whereas dense material could be advantageous in cases where a specific selectivity is desired.

This article investigates the absorption of hydrogen sulfide thanks to hydrophobic microporous hollow fiber membrane modules operated in a nonwetted mode with the gas flowing in the fiber side and the liquid in the shell. The motivations of this study are the following:

(i) Hydrogen sulfide being a toxic compound which is difficult and risky to manipulate, a very limited number of absorption of this compound with membrane contactors are reported.[2,10,11–16]

(ii) Previous papers with membrane contactors remain restricted to hydrogen sulfide absorption in chemical aqueous solutions (such as sodium carbonate, sodium hydroxide).[2,10,11–16] We report hereafter, for the first time, experimental results with absorption in water. This strategy can be of interest in order to limit the use of chemicals and prevent the need a regeneration step of the absorption liquid. Nevertheless, the absence of a chemical reaction in the liquid will have a significant influence on the mass transfer process. Consequently, a dedicated modeling analysis will be required. Thus, predicted and experimental results will be compared according to a numerical simulation in this work.

(iii) Absorption studies with traces of H_2S are scarce. For odor removal and toxicity guidelines, 100 ppm is considered as the maximum acceptable limit.[10] For that reason, this level of concentration has been taken as the inlet feed concentration in this study to evaluate the potential of water absorption with trace concentrations.

(iv) The prediction of the mass-transfer resistance on the external part of the membrane (i.e. in the extra capillary space) is known to be problematic.[9,11] Fiber geometry and packing fraction play a key role but the numerous correlations that have been reported up to now remain controversial. To that respect, two different membrane modules, showing different packing ratios, have been investigated in this study to investigate the influence of module design on mass-transfer performances.

Theoretical Background

A membrane contactor is a process that achieves gas–liquid (or liquid–liquid) mass transfer by passing the fluid to be scrubbed on the opposite side of the absorbing fluid of a microporous membrane.

The contaminated gas may flow in the tube or shell side, in concurrent or countercurrent flow with the solvent stream. The membranes could be hydrophilic or hydrophobic, that is pores could be gas-filled (dry) or liquid-filled (wet).

The gas–liquid interface is at the pore mouth of the membrane since the liquid and gas phases are flowing on each side of the membrane without any phase dispersion on both side, and this is achieved by a careful control of the pressure difference across the membrane barrier.

Two operating modes depending on the gas and absorbent pressure on either tube or shell side of the membrane-based gas–liquid contactor can be considered, namely the wetted and nonwetted (dry) modes.

In the wetted mode (Figure 1), the gas pressure P_g has to be higher than that of the liquid to prevent the latter from dispersing as drops into the gas phase. In this mode, the pores of the membrane are filled of liquid, and the absorbent, which flows on one side, wets spontaneously the hydrophilic membrane, while gas is flowing on the other side of the

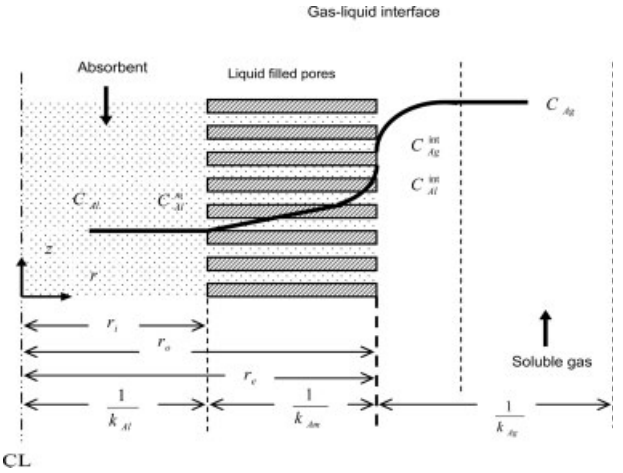

Figure 1. Wetted mode of a hollow fiber membrane contactor.

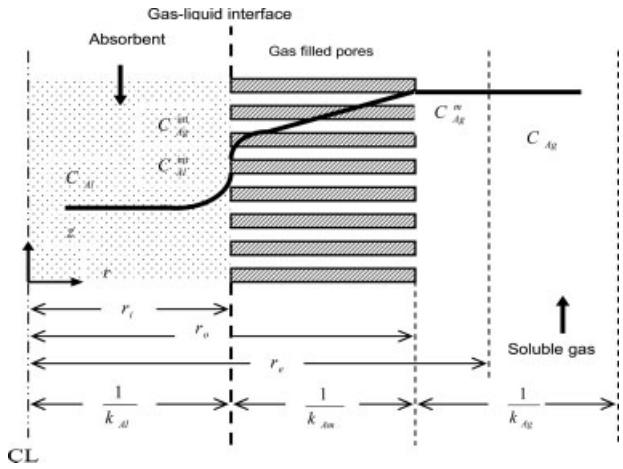

Figure 2. Non wetted mode of a hollow fiber membrane contactor.

membrane. The gas–liquid interface is at the pore mouth of the hydrophilic membrane on the gas side.

Conversely, in the nonwetted (dry) mode (Figure 2), the liquid absorbent does not wet the membrane whose pores are filled of gas. Besides, the gas pressure P_g has to be lower than that of the liquid in order to prevent any dispersion of gases in the liquid in form of bubbles. The absorbent does not cross the membrane pore mouth unless the liquid pressure exceeds a certain critical value. The gas liquid interface is at the pore mouth of the hydrophobic membrane on the liquid side.

The preference of one operation mode on the other is dictated by the importance of the chemical reaction accompanying the absorption. When the absorption is simply physical, the nonwetted mode is suitable to take advantage of the higher diffusivity in the gas phase, hence the mass transfer is controlled by the liquid phase. However, when a fast or instantaneous chemical reaction is taking place in the liquid phase, the wetted mode is indicated, and consequently a gas phase mass-transfer control.

Hence, as depicted in Figures 1 and 2, we have three mass transfer resistances in series: the gas boundary layer film, the membrane stagnant layer, and the liquid boundary layer film resistances. Since, in the nonwetted mode, the membrane pores are gas-filled, the gas phase mass-transfer resistance is likely to be more important than that in the liquid phase, except in the case where a chemical reaction is accompanying the physical absorption or when the gas solubility is not high.

Unlike the classical membrane applications (reverse osmosis, ultrafiltration, microfiltration, gas permeation, etc.), the separation driving force is the concentration gradient rather than a pressure gradient.

As shown in Figures 1 and 2, and based on the driving forces of the concentration differences, the molar mass transfer flux J_A of specie A is depicted as:

$$J_A = k_{Ag}(C_{Ag} - C^m_{Ag}) = k_{Am}(C^m_{Ag} - C^{int}_{Ag}) = k_{Al}(C^{int}_{Al} - C_{Al}) = K_{ov}\Delta C_A \quad (1)$$

Assuming the system operated at steady state, and gas and liquid at equilibrium at the membrane wall, the concentration profile is discontinuous at the membrane interface in both wetted and dry mode, according to Henry's equilibrium law.

In the case of a hydrophobic (nonwetted mode) membrane, with the liquid phase flowing on the tube side, no chemical reaction, with the driving force based on the gas phase concentration, the overall mass-transfer coefficient in series is:

$$\frac{1}{K_{ov}d_i} = \frac{1}{k_{Ag}d_o} + \frac{1}{k_{Am}d_{lm}} + \frac{1}{Hk_{Al}d_i} \quad (2)$$

A complete set of equations has been detailed by Sirkar[17] and explicitly reviewed by Boucil et al.[18]

K_{ov}, the overall mass-transfer coefficient, is calculated by the following expression:

$$K_{ov} = \frac{V}{A_T}\ln\left[\frac{C_{Agi}}{C_{Ago}}\right] \quad (3)$$

It is clearly seen from the above equation that the magnitude of the Henry's constant is a preponderant factor in the mass-transfer resistance control. For the absorption of gas specie with low H value, through a hydrophobic membrane, both the gas film and the membrane layer resistances are negligible; consequently, the mass transfer is controlled by the liquid film layer resistance.

Inversely, with a high H and a hydrophilic membrane, the gas boundary layer resistance is negligible and for a hydrophobic membrane mass transfer is mainly controlled by the boundary layer gas resistance.

The above observations are obvious in the sense that the absorption of gas specie with a high H has a higher affinity for the liquid phase, where a lower mass-transfer resistance is encountered. On the other hand, a substantial liquid film layer resistance is expected for low H gas specie.

In general, the pores that are filled by water, gas or both depend on the operating pressure, surface tension and contact angle between the two phases as reported by Mahmud et al.[19]

Experimental Section

The polypropylene made hollow fiber cartridges used in this study, whose geometrical properties are shown in Table 1, were supplied by Intersep (Wokingham, Berks, U.K.) and are similar to those used by Boucil et al.[18] Module I has a higher number of fibers than a larger contact surface area. The membrane specifications that were not supplied by the manufacturer have been estimated. The inner contact area stands for the total surface area based on the inner fiber diameter. The packing fraction is the ratio of the total outer diameter fiber volume to the shell volume. The surface to volume fraction is the ratio of the active surface area to the shell volume.

The built experimental set-up is shown in Figure 3. The gas and liquid phase, separated by the membrane wall, are circulated on a countercurrent flow pattern. Demineralized water (pH 7) was used as absorption liquid. The laboratory set-up was run (for both contactor modules) at different gas flow rates, circulating the gas continuously inside the fiber bundle, and the liquid batch-wise in the shell of the contactor. The hydrogen sulfide, a reagent grade supplied by BOC, received with a 1000 ppm v/v concentration, is diluted into air and the concentration broken down to 100 ppm v/v,

Table 1. Specifications of the HF Contactors Used is this Study

Characteristics	Module I (Close Packed)	Module II (Wide Spaced)	Source
Fibers material	Polypropylene	Polypropylene	Manufacturer
Fiber inner diameter (μm)	330	330	Manufacturer
Fiber outer diameter (μm)	360	360	Estimated
Thickness δ (μm)	15	15	Estimated
Average pore size r_p (μm)	0.06	0.06	Manufacturer
Porosity ε	0.6	0.6	Manufacturer
Number of fibers	1930	120	Estimated
Active module length (mm)	200	200	Manufacturer
Shell inner diameter (mm)	35	6	Estimated
Inner contact area (m^2)	0.40	0.0248	Manufacturer
Outer contact area (m^2)	0.4363	0.0271	Estimated
Packing fraction	0.204	0.432	Estimated
Shell side volume fraction	0.796	0.568	Estimated
Surface to volume fraction (m^2/m^3)	2400	4387	Estimated

which is equivalent to 8.314×10^{-6} moles/cm^3 at a 15-psig inlet gas pressure. The gas flow rate is measured by a gas flow meter, and the inlet and outlet gas pressures are controlled by pressure gages (0–30 psig).

Since we operate the absorption module on a nonwetted mode, the liquid pressure was carefully maintained at 15 psig, and the gas phase pressure at 10 psig.

The inlet and outlet gas mixture concentrations were controlled by means of a Custodian gas detector, supplied by Crocown Detection Instruments (Oxfordshire, U.K.), after which the outlet gas is vented through the exhaust hood. The accuracy of this probe is 1 ppm v/v in a range of 50 ppm.

Mathematical Model

The mass transport process is diffusional in the radial direction and convective in the longitudinal direction.

A theoretical model based on the second Fick's law is developed to describe the absorption of gas (H_2S) into an absorbent (water), to predict the outlet gas concentration as a function of the velocity of the absorbent in the gas side of the contactor module.

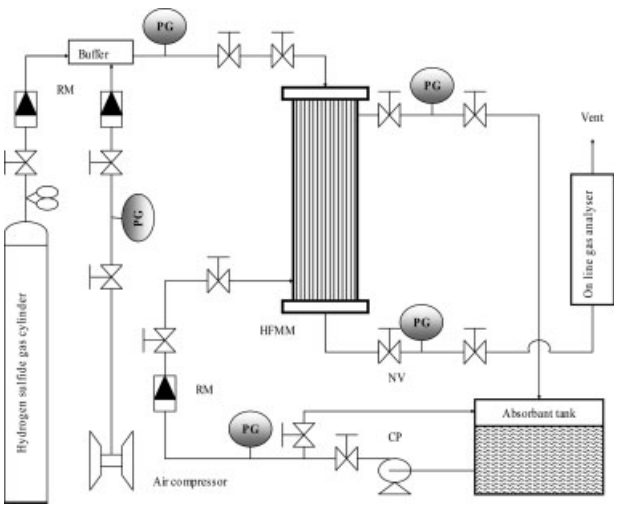

Figure 3. Experimental laboratory rig set-up.

Assuming the following valid assumptions:

(1) Isothermal conditions and ideal gas behavior (which can be checked according to corresponding state computations, for instance[20])

(2) Fully developed laminar flow in the fiber side

(3) Steady state operated system

(4) Negligible axial and angular concentrations gradients

(5) Negligible convective transport in the angular and radial directions

(6) Constant gas and liquid pressures

The mass-transfer continuous equation in cylindrical coordinates for specie i is as shown in Figure 4:

$$v_z \frac{\partial C_{Ag}}{\partial z} = D_{Ag}\left[\frac{1}{r}\frac{\partial}{\partial r}\left(r\frac{\partial C_{Ag}}{\partial r}\right)\right] + (R_A) \tag{4}$$

The hydrolysis reactions accompanying the physical diffusion of the gas (Table 2) through the membrane are:

$$H_2S + H_2O^{pH=7.04} \Leftrightarrow H_3O^+ + HS^-$$

$$HS^- + H_2O^{pK=12.9} \Leftrightarrow H_3O^+ + S^{2-}$$

For low pH values, and because of the very low values of the equilibrium constants (instantaneous chemical reactions) of both hydrolysis reactions, the formation of HS^- could be neglected. Then operating at a low range of pH values, the absorption is simply a physical transport of H_2S as observed by Hinz and Walin.[23]

When the contaminated gas is flowing into the fiber bore, and assuming a laminar flow and a fully developed parabolic velocity distribution profile in the cylindrical fiber bore, the velocity is expressed as:

$$v_z(r) = 2\bar{v}_z\left[1 - \left(\frac{r}{r_i}\right)^2\right]$$

Substituting the velocity expression into the mass transport equation yields:

$$2\bar{v}_z\left[1 - \left(\frac{r}{r_i}\right)^2\right]\frac{\partial C_{Ag}}{\partial z} = D_{Ag}\left[\frac{1}{r}\frac{\partial}{\partial r}\left(r\frac{\partial C_{Ag}}{\partial r}\right)\right] \tag{5}$$

The concentration profile is symmetrical around the center of the fiber bore, and the specie concentration in the shell

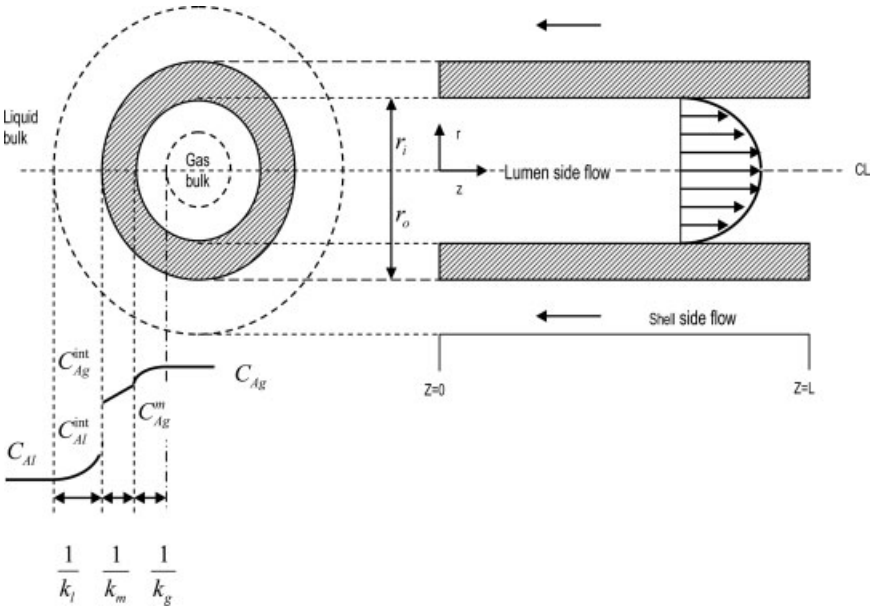

Figure 4. Flow configuration and mass-transfer resistances profiles.

side of the contactor is the gas–liquid interface concentration when the gas is flowing inside the fibers. Besides, the feed gas concentration is known at the module inlet for both circulation paths. Therefore, the above governing partial differential equations are subject to the following initial and boundary condition:

$$\text{at } z = 0, \quad C_{\text{Ag}} = C_{\text{Agi}} \quad \text{for any} \quad r_i \geq r \geq 0 \tag{6}$$

$$\text{at } r = 0, \quad \frac{\partial C_{\text{Ag}}}{\partial r} = 0 \quad \text{for any } l \geq z \geq 0 \tag{7}$$

$$\text{at } r = r_i, \quad D_{\text{Ag}} \frac{\partial C_{\text{Ag}}}{\partial r} = K_{\text{ext}} \left[C_{\text{Ag}}^{\text{int}} - C_{\text{Ag}}^{r=r_i} \right] \quad \text{for any } l \geq z \geq 0 \tag{8}$$

The reaction between H_2S and water being instantaneous, its concentration $C_{\text{Ag}}^{\text{int}}$ at the membrane–liquid interface could be neglected.

The outlet gas concentration C_{Ago} used for the calculation of the overall mass-transfer coefficient K_{ov} is determined as a "mixing cup" concentration given by Skelland[24] as:

$$C_{Ago} = \frac{\int_0^{r_i} 2\pi r v_z(r) C_{\text{Ag}} dr}{\int_0^{r_i} 2\pi r v_z(r) dr}$$

To generalize the results of this study, and simplify the governing equation along with its initial and boundary conditions it is subject to, the following dimensionless variables are introduced:

$$\xi = \frac{r}{r_i}, \quad \varsigma = \frac{z}{l}, \quad \Phi_{\text{Ag}} = \frac{C_{\text{Ag}}}{C_{\text{Agi}}} \tag{9}$$

Introduction of these new variables into Eqs. 5 through 8 and after simplifications and rearrangements yields to:

$$\frac{\partial \Phi_{\text{Ag}}}{\partial \varsigma} = 2\left(\frac{Dl}{\bar{v}_z d_i^2}\right)\left[\left(\frac{1}{1-\xi^2}\right)\left\{\frac{1}{\xi}\frac{\partial}{\partial \xi}\left(\xi \frac{\partial \Phi_{\text{Ag}}}{\partial \xi}\right)\right\}\right] \tag{10}$$

Hence, the initial and boundary conditions will simplify to:

$$\text{at } \varsigma = 0, \quad \Phi_{\text{Ag}} = 1 \tag{11}$$

$$\text{at } \xi = 0, \quad \left.\frac{\partial \Phi_{\text{Ag}}}{\partial \xi}\right|_{\xi=0} = 0 \tag{12}$$

$$\text{at } \xi = 1, \quad \left.\frac{\partial \Phi_{\text{Ag}}}{\partial \xi}\right|_{\xi=1} = -\frac{Sh_{\text{ex}}}{2} \Phi_{\text{Ag}}\big|_{\xi=1} \tag{13}$$

where the term $\frac{\bar{v}_z d_i^2}{Dl}$ is the dimensionless Graetz number based on the internal fiber diameter, and related to the dimensionless Reynolds and Schmidt numbers as: $Gr = \text{Re}\, Sc d_i/l$.

The Sh_{ex} is the external dimensionless Sherwood number defined as $Sh_{\text{ex}} = K_{\text{ext}} d_i / D_{\text{Ag}}$ where the K_{ext} stands for the combined mass transfer in the gas phase and the membrane and calculated as $\frac{1}{K_{\text{ext}}} = \frac{1}{k_{\text{Am}}} + \frac{1}{k_{\text{Ag}}}$. Kreulen et al.[25] have mentioned that in porous structures, the diffusion prevails over convection and the mass transfer through the membrane can be calculated as follows:

$$\frac{1}{k_{\text{Am}}} = \frac{\delta\tau}{D_{\text{Am}}\varepsilon} = \frac{\delta\tau}{\varepsilon}\left(\frac{1}{D_{\text{Ag}}} + \frac{1}{D_{\text{AK}}}\right) \tag{14}$$

The D_{Am} is the diffusion coefficient in the membrane micropores, and is a combination of the continuum or molecular

Table 2. Gas Parameters Used is this Study

Gas Parameter	Value	Source
Diffusivity D_{Al} of H_2S in water	$2.10 \times 10^{-9}\ m^2/s$	Haimour et al.[21]
Diffusivity D_{Ag} of H_2S in air	$1.65 \times 10^{-5}\ m^2/s$	Diaz et al. [22]

diffusion D_{Ag} which is determined by the different molecules interactions, and the Knudsen diffusion D_{AK} when the molecules interactions with the pore's walls are taken into account.

The Knudsen diffusion is expressed as: $D_{AK} = \frac{2r_p}{3}\sqrt{\frac{8\Re T}{\pi M_A}}$.

It has been reported by Kreulin et al.[25] that the Knudsen diffusion is considerable only for small pore diameters ($r_p < 0.05$ μm). Furthermore, Prasad and Sirkar (1985) have related the tortuosity to the porosity as $\tau = (2-\varepsilon)^2/\varepsilon$, whereas, Dindore et al.[10] have estimated the porosity to tortuosity ratio as 0.42 for microporous polypropylene hollow fiber membranes.

The outlet mixing cup concentration rewritten in a dimensionless form is:

$$\Phi_{Ago} = 4\int_0^1 \xi(1-\xi^2)\Phi_{Ag}d\xi \tag{15}$$

The extent of the soluble gas removal η which expresses the percentage of the solute in the gas stream that was recovered is defined as:

$$\eta = \frac{C_{Agi} - C_{Ago}}{C_{Agi}} = 1 - \Phi_{Ago} \tag{16}$$

Analytical Solution

The separation of variables method is used to solve this problem. If we let $\Phi(\xi,\varsigma) = R(\xi)Z(\varsigma)$, the governing partial differential equation gives rise to two separate ordinary differential equations, namely:

$$\frac{dZ}{Z} = -\frac{2\beta^2}{Gr}d\varsigma \tag{17}$$

$$\xi\frac{d^2R}{d\xi^2} + \frac{dR}{d\xi} + \beta^2\xi(1-\xi^2)R = 0 \tag{18}$$

where β^2, a real positive number, represents the eigenvalues of the system.

The solution of Eq. 17 is

$$Z(\varsigma) = C_1\exp\left[-\frac{2\beta^2\varsigma}{Gr}\right] \tag{19}$$

where C_1 is an arbitrary integration constant.

Making use of the transformations on both the dependant variable $u = \beta\xi^2$ and on the independent one $R(u) = e^{-\frac{u}{2}}S(u)$, the differential Eq. 18 is transformed to:

$$u\frac{d^2S}{du^2} + (1-u)\frac{dS}{du} - \left(\frac{1}{2} - \frac{\beta}{4}\right)S = 0 \tag{20}$$

which is known as Kummer's equation[26] and admits, under the boundary condition of symmetry, (12) the solution:

$$R(\xi) = \exp\left(-\frac{\beta\xi^2}{2}\right){}_1F_1\left(\frac{1}{2} - \frac{\beta}{4}; 1; \beta\xi^2\right) \tag{21}$$

${}_1F_1$ is the Kummer Hypergeometric function of the first kind and defined by:

$${}_1F_1(a;b;x) = \sum_{i=0}^{\infty}\frac{a_i x^i}{b_i i!} = 1 + \frac{ax}{b} + \frac{(a)_2x^2}{(b)_2 2!} + \frac{(a)_3x^3}{(b)_3 3!} ..... + \frac{(a)_i x^i}{(b)_i i!} \tag{22}$$

with $(a)_i = a(a+1)(a+2).....(a+i-1)$ and $(b)_i = b(b+1)\ (b+2).....(b+i-1)$.

The eigenvalues β_i are the roots of the equation resulted from the application of the second boundary condition:

$$\left(\frac{Sh}{2} - \beta_i\right){}_1F_1\left(\frac{1}{2} - \frac{\beta_i}{4}; 1; \beta_i\right) + 2\beta_i\left(\frac{1}{2} - \frac{\beta_i}{4}\right) \times {}_1F_1\left(\frac{3}{2} - \frac{\beta_i}{4}; 2; \beta_i\right) = 0 \tag{23}$$

The system being linear, a general solution is obtained by superposition:

$$\Phi(\xi,\varsigma) = \sum_{i=1}^{\infty} C_{2i}\exp\left(-\frac{2\beta_i^2\varsigma}{Gr}\right)\exp\left(\frac{\beta_i\xi^2}{2}\right) \times {}_1F_1\left(\frac{1}{2} - \frac{\beta_i}{4}; 1; \beta_i\xi^2\right) \tag{24}$$

The integration coefficients C_{2i} of the above general solution are obtained by applying the initial condition[18] and afterwards by making use of the orthogonal properties of the Sturm–Liouville system:

$$C_{2i} = \frac{\frac{1}{\beta_i}\exp\left(-\frac{\beta_i}{2}\right)\left[{}_1F_1\left(\frac{1}{2}-\frac{\beta_i}{4};1;\beta_i\right) - \left(1-\frac{\beta_i}{4}\right){}_1F_1\left(\frac{3}{2}-\frac{\beta_i}{4};2;\beta_i\right)\right]}{\int_{\xi=0}^{\xi=1}\left\{\xi(\xi-\xi^2)\exp(-\beta_i\xi^2)\left[{}_1F_1\left(\frac{1}{2}-\frac{\beta_i}{4};1;\beta_i\xi^2\right)\right]^2\right\}d\xi} \tag{25}$$

It is worth noting that the eigenvalues β_i of the algebraic Eq. 23 and the integral in the C_{2i} denominator are evaluated by any suitable numerical techniques.

Numerical Solution Procedure

Solving analytically this problem is a quite tedious task. However, many numerical techniques can be used to solve this nonlinear partial differential equation, such as the finite difference discretization, quasi-linearization techniques, and the orthogonal collocation methods.

The orthogonal collocation, introduced by Villadsen and Stewart,[27] is a technique categorized as a method of weight residuals and has been shown by Finlayson[28] to be superior in some respects to the finite difference approaches and yield more accurate results with less computational effort compared with the conventional methods. Extensive and successful applications of this method to dynamic simulations of chemical processes have been made.[29–31]

The dependant dimensionless variable Φ_{Ag} is approximated as:

$$\Phi_{Ag} = \sum_{j=1}^{n+2} l_i(\xi_j)\Phi(\xi_j,\varsigma) \tag{26}$$

where $l_j\ (\xi_j)$, $j = 1, n+2$ are the interpolation polynomials and $\Phi(\xi_j, \varsigma)$ is the value of concentration Φ_{Ag} at collocation points $\xi = \xi_i$ and space coordinate ς. The $n+2$ term comes from the fact that $\xi = 0$ and $\xi = 1$ are also roots of the approximation polynomial.

The collocation points are chosen to be the zeros of the polynomials $P_n^{(\alpha,\beta)}(\xi)$ and the boundary points. These approx-

imation polynomials are described by the orthogonality relation as:

$$\int_0^1 \xi^{\alpha}(1-\xi)^{\beta} P_n^{(\alpha,\beta)}(\xi) P_m^{(\alpha,\beta)}(\xi) d\xi = 0$$

where $\xi^{\alpha}(1-\xi)^{\beta}$ is the weight function with α, $\beta > -1$. The choice of α, β of the weighting function determines the type of polynomials used (Legendre, Lagrange, etc.), and consequently the location of the collocation points. Note that for cylindrical coordinates, the more suitable values for α and β are respectively 1 and 1.5.

Differentiating Eq. 26 gives:

$$\frac{\partial \Phi_j}{\partial \xi} = \sum_{j=1}^{n+2} A_{i,j} \Phi_j(\xi_j, \varsigma) \quad \text{with} \quad A_{i,j} = \frac{dl_j}{d\xi} \text{ at } \xi = \xi_i \qquad (27)$$

$$\frac{\partial^2 \Phi_j}{\partial \xi^2} = \sum_{j=1}^{n+2} B_{i,j} \Phi_j(\xi_j, \varsigma) \quad \text{with } B_{i,j} = \frac{d^2 l_j}{d\xi^2} \text{ at } \xi = \xi_i \qquad (28)$$

where $A_{i,j}$ and $B_{i,j}$ are the weights for the first and second spatial derivative at ξ_i respectively.

The normal radial position ξ is defined to be 0 at the center of the fiber bore and 1 at the surface of the inner radius. Hence, the collocation points are numbered from 1 to $n + 2$ with n interior collocation points and two end points.

Inserting Eqs. 27 and 28 into the governing partial differential equation yields to:

$$\frac{d\Phi_i}{dz} = \frac{2}{Gr(1-\xi_i^2)} \left\{ B_{ij}\Phi_1 + \sum_{j=2}^{n+1} B_{i,j}\Phi_j + B_{i,n+2}\Phi_{n+2} + \frac{1}{\xi_i} \times \left[A_{i1}\Phi_1 + \sum_{j=2}^{n+1} A_{i,j}\Phi_j + A_{i,n+2}\Phi_{n+2} \right] \right\} \qquad (29)$$

The terms Φ_1 and Φ_{n+2} in the above expression are determined by means of the discretization of the boundary conditions (12) and (13) which are $\sum_{j=1}^{n+2} A_{1,j}\Phi_j = 0$ and $\sum_{j=1}^{n+2} A_{n+2,j}\Phi_j = -\frac{Sh}{2}\Phi|_{\xi=1}$, and rewritten respectively as:

$$A_{1,1}\Phi_1 + A_{1,n+2}\Phi_{n+2} = -\sum_{j=2}^{n+1} A_{1,j}\Phi_j$$

$$A_{n+2,1}\Phi_1 + \left(A_{n+2,n+2} + \frac{Sh}{2} \right)\Phi_{n+2} = -\sum_{j=1}^{n+2} A_{n+2,j}\Phi_j$$

The solution of the couple of algebraic equations yields the expression of Φ_1 and Φ_{n+2} that are substituted back into the governing equation to give:

$$\frac{d\Phi_i}{dz} = \frac{2}{Gr(1-r_i^2)} \left[\sum_{J=2}^{n+1} B_{i,j}\Phi_j + \frac{1}{\xi_i} \sum_{j=2}^{n+1} A_{i,j}\Phi_j + \frac{\mathrm{ANI} \sum_{j=2}^{n+1} A_{1,j}\Phi_j + \mathrm{AN2} \sum_{j=2}^{n+2} A_{n+2,j}\Phi_j}{\mathrm{DN}} \right] \qquad (30)$$

where:

$$\mathrm{AN1} = \left(B_{i,n+2} + \frac{A_{i,n+2}}{\xi_i} \right) A_{n+2,1} - \left(B_{i,1} + \frac{A_{i,1}}{\xi_i} \right) \times \left(A_{n+2,n+2} + \frac{Sh}{2} \right)$$

$$\mathrm{AN2} = \left(B_{i,1} + \frac{A_{i,1}}{\xi_i} \right) A_{1,n+2} - \left(B_{i,n+2} + \frac{A_{i,n+2}}{\xi_i} \right) A_{1,1}$$

$$\mathrm{DN} = \left(A_{n+2,n+2} + \frac{Sh}{2} \right) A_{1,1} - A_{1,n+2}A_{n+2,1}$$

At this moment, the problem to be solved has been reduced to the simultaneous solution of n ordinary differential equations at each collocation point ξ_i, n being the number of interior collocation points. It goes without saying that the higher is n, the more accurate will be the results, but the more computing effort and more time consuming.

Results and Discussions

The set of n ordinary differential Eq. 30, was simultaneously solved by a Runge–Kutta fifth order algorithm. The discretized ODE at the surface of the fiber is henceforth integrated from the initial condition $\varsigma = 0$, to the contactor exit at $\varsigma = 1$, which is in fact the simulated dimensionless outlet concentration Φ_{Ago}. The numerically simulated results are plotted in terms of *Gr* vs. *Sh*.

The performance of the two hydrophobic hollow fiber membrane modules, the close packed (Module I with large contact surface area) and the wide spaced (Module II with lower surface area), has been studied theoretically and experimentally for the absorption of H_2S into water.

As shown earlier, k_{Am} can be independently estimated from Eq. 14 knowing the pore properties for the hydrophobic membrane.

The performance of the hollow fiber membrane module was theoretically studied and the depletion extent η was plotted against *Gr* for different *Sh* values as shown in Figure 5. It can be seen from this plot that the contaminant gas removal improves as the feed gas velocity in the fiber bore decreases. The impact of the gas velocity expressed as the *Gr* number on the mass-transfer coefficient expressed as the

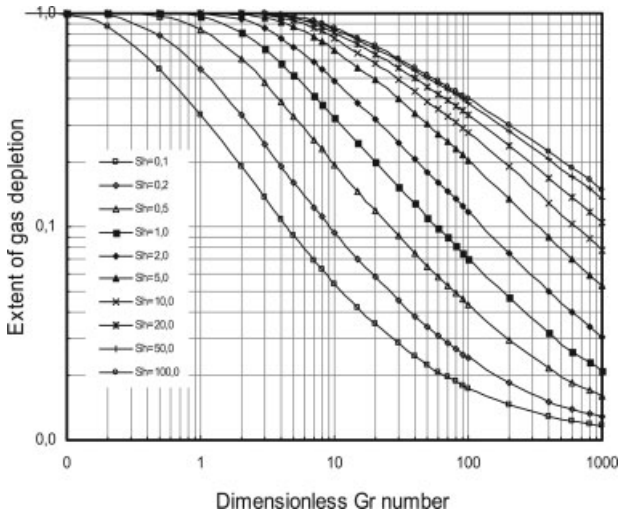

Figure 5. Simulated effect of *Sh* number on gas depletion.

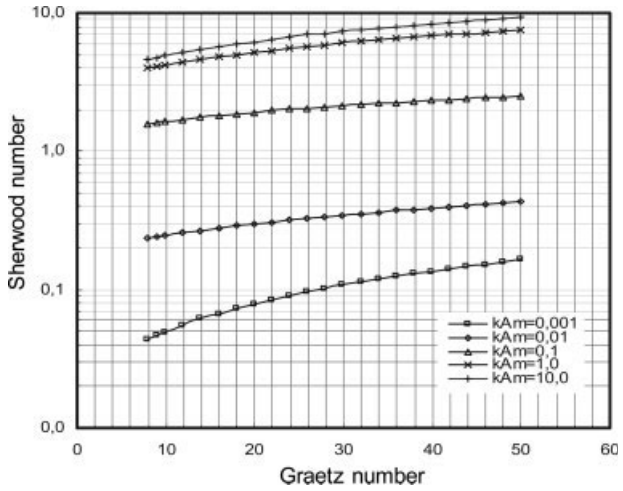

Figure 6. Simulated *Sh* number as a function of *Gr* for different k_{Am}.

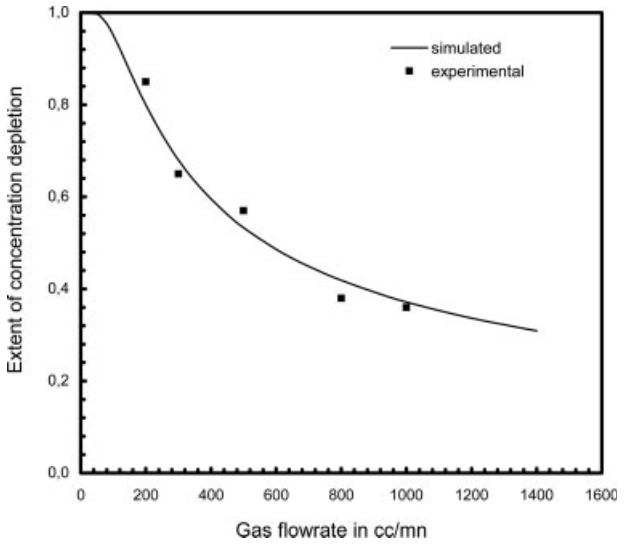

Figure 7. Experimental and simulated extent of concentration depletion for different gas flow rates for Module I.

Sh number has been theoretically studied. Figure 6 plots the effect of *Gr* on *Sh* at different membrane resistances and exhibits that the overall mass transfer K_{ov} is independent of the gas velocity for higher k_{Am}. For negligible membrane resistances ($k_{Am} \geq 10$ *m/s*), the variation of *Sh* with *Gr* number is insignificant.

Figure 5, a graph drawn from numerically simulated results, could be used to predict the design parameters of the hollow fiber contactor module knowing the operating conditions. In fact, for a specific gas and membrane morphology, one can determine the membrane resistance $1/k_{Am}$ through Eq. 14, and consequently the external Sherwood number Sh_{ex}. The dimensionless extent η, is obtained from Eq. 16 for a fixed inlet and desired outlet gas concentration, for which a value of the *Gr* number is generated from Figure 5 for the aforementioned Sh_{ex}. In consequence, and from the definition of Gr, for a known gas flow rate and length of fibers, the diameter and number of fibers could be easily estimated to meet the performance requirements of the contactor module.

The extent of gas depletion expresses the recovery efficiency which is one of the most important properties of HFM separation process and is expressed and determined by Eq. 16 as the percentage of H_2S in the gas stream that was recovered through the absorption process.

Figures 7 and 8 illustrate the H_2S extent of concentration depletion in the gas outlet stream as a function of gas flowrate. Experimental data and numerical simulation are presented for both HFM Modules I and II.

These figures show that a maximum acid gas removal of 85% has been achieved at a gas flow rate of 200 cm^3/mn with Module I and 89% at 10 cm^3/mn for Module II. The contact surface area, which could be increased by using a larger number of fibers or by increasing the fiber bundle length in the module, permits an efficient diffusional mass-transfer. Consequently, because Module I has a larger contact surface area, a higher amount of H_2S is present in the outlet gas stream in Module II compared with Module I for the same gas flow rate. The model solution agrees with the experimental data with a maximum deviation of up to 12% due mainly to the estimation of the porosity to tortuosity ratio ε/τ involved in the determination of the membrane resistance k_{Am}. The essential reason to this difference is probably that the membrane assumed to be completely dry was partially wetted as a result of the gas and liquid fluctuating pressures.

Figures 9 and 10 compare the same experimental data drawn as *Sh* number vs. *Gr* number with the numerically simulated results for both modules. In this plot, the simulated results as well as the experimentally generated are in a good agreement with the theoretical truncated correlation known as the Levêque solution ($Gr = 1.62\ Sh^{1/3}$).

Figures 11 and 12 exhibit the effect of the gas velocity in the fiber bore on the overall mass-transfer coefficient for both membrane contactors. The theoretical and experimental values have been calculated by means of Eq. 3. Both figures show that the overall mass-transfer coefficient vary very slightly with the velocity in the gas phase.

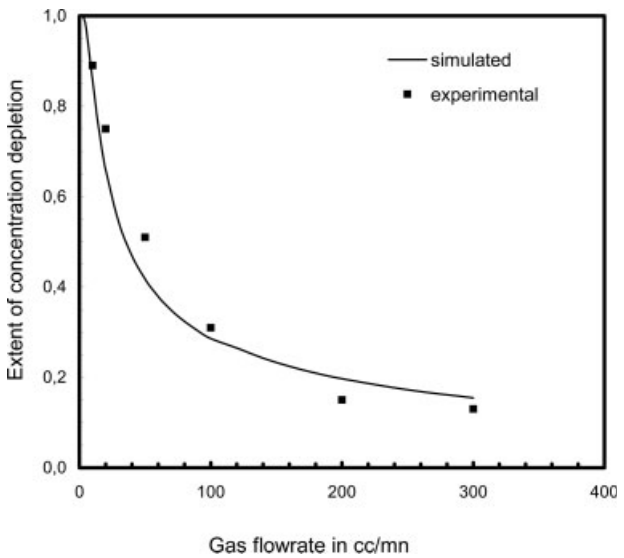

Figure 8. Experimental and simulated extent of concentration depletion for different gas flow rates for Module II.

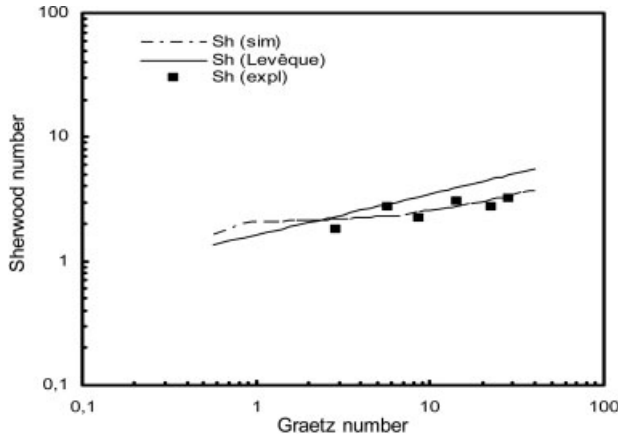

Figure 9. Comparison of simulated *Sh* with Levêque solution for Module I.

The gas flow rate is probably the most important operating variable in the gas–liquid membrane contactor because, in general, it has an obvious influence on the mass-transfer rate of H_2S. It is observed from both Figures 11 and 12, that the H_2S overall mass-transfer rate increases slightly whith an increasing gas flow rate.

This is very likely due to the fact that the boundary layer thickness of the gas phase in the lumen side decreases with the increasing gas flow rate, which has an effect of decreasing the mass-transfer resistance of the gas phase resulting in a slight increase in the mass diffusion.

The numerically calculated results are in reasonable agreement with the experimentally generated data, especially for Module I, Module II having a narrow cartridge has shown channeling problems during its operation. The deviation of the laboratory collected data from the simulated results is mainly due to experimental errors and the uncertainty of the hypothetical assumptions involved in the theoretical model development.

Conclusion

The experimental studies conducted with the polypropylene HFMCs have demonstrated that this technology can effectively

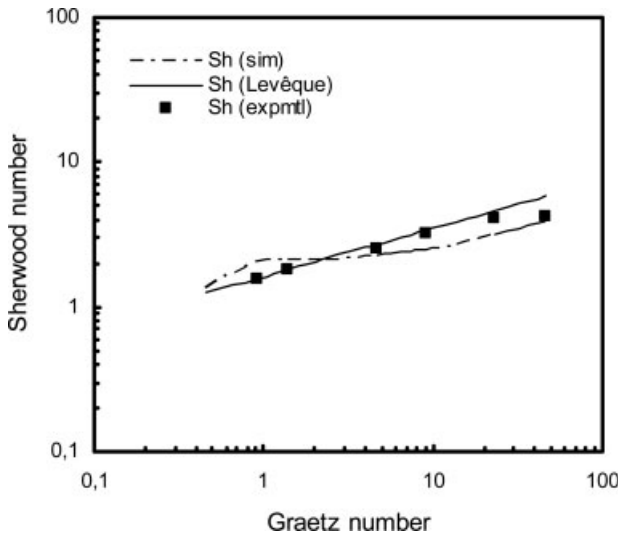

Figure 10. Comparison of simulated *Sh* with Levêque solution for Module II.

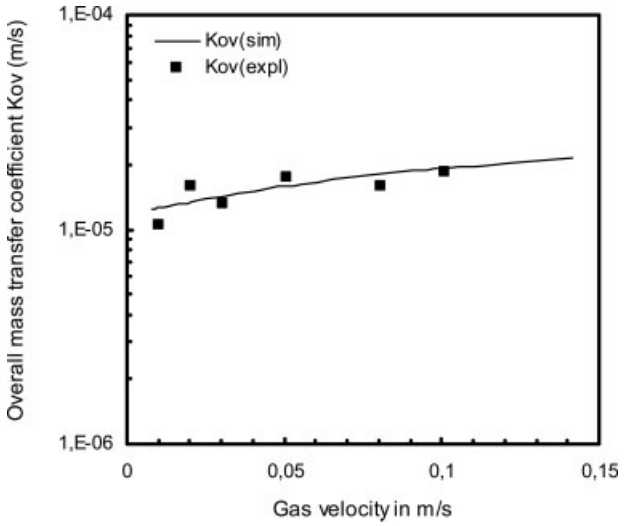

Figure 11. Simulated and experimental overall mass-transfer coefficient for Module I.

remove H_2S with substantial efficiencies of up to 89% for inlet concentrations of 100 ppm v. This study has also shown that the gas–liquid absorption of H_2S in a hollow fiber contactor is mostly membrane resistance controlled. The overall mass-transfer coefficient of the absorption process are in the same order of magnitude for the two modules and were found to vary between 1.0 and 1.5 $\times$ 10^{-5} m/s. The overall mass-transfer coefficient was found to vary as a linear function of the gas velocity with an almost negligible slope, but was insensitive to the inlet gas concentration. The membrane and/or gas phase resistance has a significant effect on this mass-transfer process. This is true for fast reactions in the liquid phase and/or considerable gas flow rates. If the overall mass-transfer resistance, $1/K_{ov}$, increases in the same extent than according to the resistance-in-series model, one may conclude that the resistance in the liquid has no substantial impact at the actual applied conditions where the mass transfer resistance in the membrane and/or gas phase is much higher.

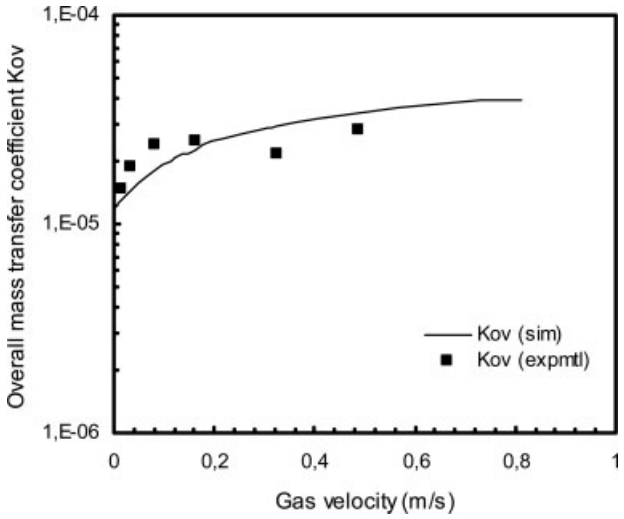

Figure 12. Simulated and experimental overall mass transfer for Module II.

The analysis of the data reveals that the performance of the hollow fiber membrane contactor is dependant on the gas velocity in the fibre lumen as well as on the module's geometry. In fact, because of its larger contact surface area, the absorption efficiency is higher in Module I compared with Module II for the same gas flow rates.

Notation

A_T = total surface area of gas liquid contact (m^2)
$A_{i,j}$ = matrix coefficients of the weight first derivative
$B_{i,j}$ = matrix coefficients of the weight second derivative
C_{Ag} = gas phase molar concentration of specie A (mol/m^3)
C_{Al} = liquid phase molar concentration of specie A (mol/m^3)
C_{Ag}^{int} = gas phase molar concentration of specie A at the membrane wall (mol/m^3)
C_{Ag}^{m} = molar concentration of specie A across the membrane barrier (mol/m^3)
C_{Al}^{int} = liquid phase molar concentration of specie A at the membrane wall (mol/m^3)
C_{Agi} = molar concentration of specie A in the gas phase at module entrance (mol/m^3)
C_{Ago} = molar concentration of specie A in the gas phase at module exit (mol/m^3)
D_{Al} = diffusion coefficient of specie A in water (m^2/s)
D_{Ag} = diffusion coefficient of specie A in air (m^2/s)
D_{AK} = continuum Knudsen diffusion coefficient of specie A (m^2/s)
d_i = inner fiber diameter (m)
d_{lm} = logarithmic mean diameter (m)
d_o = outer fiber diameter (m)
Gr = dimensionless Graetz number
H = dimensionless Henry's law constant (–)
J_A = molar mass-transfer flux of specie A (mol/s)
k_{Ag} = gas film mass-transfer coefficient of specie A (m/s)
k_{Al} = liquid film mass-transfer coefficient of specie A (m/s)
k_{Am} = membrane mass-transfer coefficient of specie A (m/s)
K_{ext} = external mass-transfer coefficient (m/s)
K_{ov} = overall mass-transfer coefficient (m/s)
M_A = solute molecular weight (kg/mol)
l = active membrane fiber length (m)
l_j = orthogonal interpolating polynomial
n = number of fiber in the bundle (–)
r = radial coordinate
r_i = inner fiber radius
r_o = outer fiber diameter
r_p = mean pore radius (m)
R = ideal gas constant (8.314 Pa.m^3 / mol °K)
Sh = dimensionless Sherwood number (–)
T = temperature in °K
V = gas flow rate (m^3/s)
$v_z(r)$ = radius dependant velocity in the z direction
$\overline{v}_z$ = mean average velocity in the fiber in the z direction (m/s)
z = longitudinal contactor coordinate

Greek letters

Φ_{Ag} = dimensionless concentration of specie A in the gas phase
Φ_{Agi} = dimensionless inlet concentration of specie A in the gas phase
Φ_{Ago} = dimensionless outlet concentration of specie A in the gas phase
ς = dimensionless longitudinal coordinate
ξ = dimensionless radial coordinate
ξ_i = collocation point
ε = fiber bundle to shell packing fraction
η = extent of gas removal
δ = membrane thickness
τ = membrane's pore tortuosity

Literature Cited

1. Esato K, Eisman B. Experimental evaluations of Gore Tex™ membrane oxygenator. *J Thor Cardiovasc Surg*. 1975;69:690–697.
2. Qi Z, Cussler EL. Microporous hollow fibers for gas absorption. *J Membr Sci*. 1985;23:321–332.
3. Cooney DO, Jackson CC. Gas absorption in a hollow fiber device. *Chem Eng Commun*. 1989;79:153–163.
4. Karoor S, Sirkar KK. Gas absorption studies in microporous hollow fiber membranes. *Ind Eng Chem Res*. 1993;32:674–684.
5. Matson SL, Lopez J, Ward WJ. Separation of gases with synthetic membranes. *Chem Eng Sci*. 1983;38:503–512.
6. Yang MC, Cussler EL. Designing hollow fiber contactors. *AIChE J*. 1986;32:1910–1916.
7. Prasad R, Sirkar KK. Dispersion-free solvent extraction with microporous hollow fiber membrane. *AIChE J*. 1988;34:177–188.
8. Sirkar KK. Membrane separation technologies: current developments. *Chem Eng Commun*. 1997;157:145–184.
9. Gabelman A, Hwang ST. Hollow fiber membrane contactors. *J Membr Sci*. 1999;159:61–106.
10. Dindore VY, Brilman BWF, Versteeg GF. Modeling cross flow membrane contactors: mass transfer with chemical reactions. *J Membr Sci*. 2005;55:275–289.
11. Criscuoli A, Drioli E, Moretti U. Membrane contactors in the beverage industry for controlling the water gas composition. *Ann N Y Acad Sci*. 2003;984:1–16.
12. Tan X, Li K, Teo WK. Odor control using hollow fiber membrane modules. *AIChE J*. 2005;51:1367–1376.
13. Wang D, Teo WK, Li K. Selective removal of trace H_2S from gas streams containing CO_2 using hollow fibre membrane modules/contactors. *Sep Pur Technol*. 2004;35:125–131.
14. Li K, Wang D, Koe CC, Teo WK. Use of asymmetric hollow fibre modules for elimination of H_2S from gas streams via a membrane absorption method. *Chem Eng Sci*. 1998;53:1111–1119.
15. Wang D, Teo WK, Li K. Removal of H_2S to ultra-low concentrations using an asymmetric hollow fibre membrane module. *Sep Pur Technol*. 2002;27:33–40.
16. Li K, Kong JF, Wang D, Teo WK. Tailor-made asymmetric PVDF hollow fibers for soluble gas removal. *AIChE J*. 1999;45:1211–1220.
17. Sirkar KK. Other new membranes. In: Ho WSW and Sirkar KK, editor. *Membrane Handbook*. New York: Van Nostrand Reinhold, 1992:885–899.
18. Boucil N, Jefferson B, Parsons SA, Judd SJ, Stuetz RM. Direct molecular hydrogen sulfide scrubbing with hollow fiber membranes. *Water Sci Technol*. 2001;44:135–142.
19. Mahmud H, Kumar A, Narbaitz RM, Matsuura T. Mass transport in air stripping process using microporous polypropylene hollow fiber: effect of toluene in aqueous feed. *J Membr Sci*. 2002;209:207–219.
20. Reid RC, Prauznitz JM, Sherwood TK. *The Properties of Gases and Liquids*. New York: McGraw-Hill, 1977.
21. Haimour N, Sandall OC. Molecular diffusivity of hydrogen sulfide in water. *J Chem Eng Data*. 1984;29:20–22.
22. Díaz M, Vega A, Coca J. Correlation for the estimation of gas-liquid diffusivity. *Chem Eng Commun*. 1987;52:271–281.
23. Hinz A, Wallin M. Individual and simultaneous desorption of H_2S and CO_2 from synthetic green liquor. *Chem Eng J*. 1999;72:63–67.
24. Skelland AHP. *Diffusional Mass Transfer*. New York: Wiley, 1974.
25. Kreulen H, Smolders CA, Versteeg GF, Vanswaaij WPM. Determination of mass transfer in wetted and non-wetted microporous membranes. *Chem Eng Sci*. 1993;48:2093–2102.
26. Slater LJ. *Confluent Hypergeometric Functions*. London: Cambridge University Press, 1960.
27. Villadsen JV, Stewart WE. Solution of boundary value problems by orthogonal collocation. *Chem Eng Sci*. 1967;22:1483–1501.
28. Finlayson BA. Packed bed reactor analysis by orthogonal collocation. *Chem Eng Sci*. 1971;26:1081–1091.
29. Kao YK, Yan Z. Dynamic modeling and simulation of simple membrane permeators. *Chem Eng Commun*. 1987;59:343–370.
30. Michelsen ML. Axial dispersion and the collocation method. *Chem Eng Sci*. 1994;1:3675–3682.
31. Tessendorf S, Gani R, Michelsen ML. Modeling, simulation, and optimization of membrane-based gas separation systems. *Chem Eng Sci*. 1999;54:943–955.

Manuscript received July 3, 2007, and revision received Sept. 24, 2007.